Lasers in Manufacturing Conference 2025

Automated inline rewelding processes based on detection of process anomalies during laser deep penetration welding

Andreas Krämer[a*], Timon Ahlers[a], Ronald Pordzik[a], Tim Radel[a,b]

[a]*BIAS – Bremer Institut für angewandte Strahltechnik GmbH, Klagenfurter Straße 5, 28359 Bremen, Germany*
[b]*MAPEX Center for Materials and Processes, Postfach 330 440, 28334 Bremen*

Abstract

During laser deep penetration welding, disturbances of the nominal process can lead to seam imperfections. Due to their possibly impairing characteristics on the mechanical properties of the seam, it is of high interest to reliably detect these defects. This can be achieved by means of sensor based inline process monitoring. While the sensor data can be employed to identify the defect location and perform post process repair work, it can also build the foundation to reweld the detected seam segments inline to enhance the seam quality and possibly eliminate necessary post process work. This study demonstrates an approach to detect provoked process anomalies during laser deep penetration welding of hidden T-joints in line and use a LabVIEW based control algorithm to utilize the scanning capabilities of the welding optic to reweld the defected seam area inline.

Keywords: multisensory process monitoring, rewelding, process control

1. Introduction

Following the strive for sustainability and high production efficiency, post process quality control tends to be a time and cost consuming bottle neck. Therefore, the demand for robust laser deep penetration welding processes rises. In automized production facilities the raw material itself can be impaired and contaminations can get entrapped within joint gaps due to insufficient cleaning procedures. Therefore the influence of oil within joint gaps was investigated by Geiger et al. (Geiger et al. 2008). Theyw found an increase in keyhole collapses and consequently an increase in seam porosity due to the oil evaporation as well as an increase in melt pool waves and melt ejection. For aluminium sheets coated with Drylube E1, Hagenlocher et al. (Hagenlocher et al. 2020) also found a significant increase in porosity. However, the origin of the pore formation by means of in-situ x-ray imaging was located well behind the keyhole. Recently, the authors investigated the influence of entrapped polystyrene particles, a common packing material, onto the seam quality and also found an increase in porosity as well as a reduction in welding depth due to a significant widening of the keyhole because of the additional evaporation of the polystyrene (Krämer et al. 2024). While monitoring the process with optical coherence tomography (OCT) and airborne sound sensoring, the ability to detect the contaminated seam segments in-situ due to the significant process anomalies was shown. The ability to detect seam imperfections in-situ offers the opportunity to react to the disturbed processes accordingly. While there is a lot of research on stabilizing the keyhole process itself and increasing the welding speed, such as by using spot in spot beam shaping (Möbus et al. 2024), there is only a very limited amount of studies regarding the effect of rewelding imperfected seam areas. Zhao et al. (Zhao and Debroy 2001) examined the effect of a second welding pass and observed a reduction in porosity. A similar behavior is known from laser polishing by remelting, which can reduce the surface near porosity (Rathmann et al. 2022; Yasa and Kruth 2011). This work therefore demonstrates the proof of concept to in-situ reweld imperfect seam segments based on the automatic detection of those areas.

* Corresponding author. Tel.: +49 421 218 58052
E-mail address: kraemer@bias.de

2. Experimental Setup and methods

The possibility of in-situ repair welding in a hidden T-joint joint configuration was investigated using multi-sensor data acquisition and an FPGA-based control system. The control system must analyze the sensor data in real time and execute repair strategies accordingly. Using the multi-sensor experimental setup with airborne sound microphone and OCT described in (Krämer et al. 2024), only the signal from the additionally integrated Kleiber KGA740-LO pyrometer was used in a first attempt since the pyrometric signal reacts in a similar way to contamination induced process anomalies but requires fewer pre-processing calculations, which eases the implementation on the FPGA. For the evaluation of the macroscopic process behavior during the contaminated segments as well as the rewelding intervention, the process was monitored by a lateral positioned Photron Nova S12 highspeed camera with a frame rate of 20 kfps. The experimental setup is displayed in Fig. 1. While the camera was fixed, the specimen was moved by a motorized linear axis.

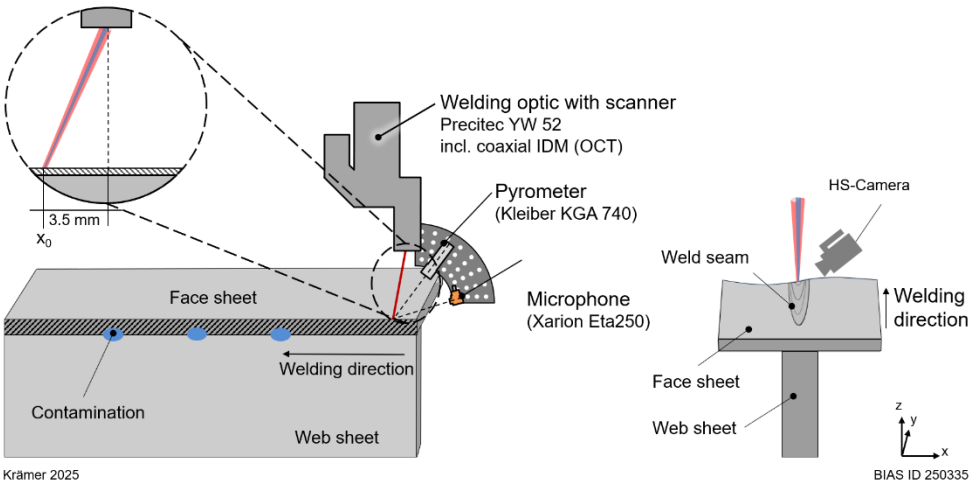

Fig. 1: Experimental Setup

For real-time detection the measurement signal is transmitted to the controller in the form of analog voltage. The controller is based on a cRIO-9030 FPGA controller from National Instruments. The voltage signal is sampled via a NI-9223 analog input card of the C series with 16 bits and a sample rate of 14 µs. The measured values are pre-processed on the FPGA using a floating average filter over 350 measured values. The averaged signal is then used to decide by means of a threshold whether a defect occurred and a corresponding reaction in the form of a rewelding process is necessary. The reaction of the system is implemented using the 1D scanner integrated in the YW52 welding optics from Precitec. For this purpose, the optics was aligned in a way so that the processing laser including the OCT measuring beam can be deflected parallel to the welding direction by $\pm$ 3.5 mm. In the nominal process, the spot is deflected 3.5 mm in the welding direction. If a defect is detected, the laser beam can be deflected backwards by up to 7 mm in order to repair the weld. The position of the scanner is specified via an analog voltage signal, which the controller outputs via an NI-9263 C-series voltage output card at the same rate of 14 µs.

For calculating the necessary jump distance, the timestamps of the threshold violations were monitored. A logic of intervention was applied to prevent controller reactions due to threshold violations during the rewelding phase. The jump distance Δs was calculated by

$$\Delta s = \Delta t \cdot v_s + s_{SF} \qquad (1)$$

with Δt representing the time difference between the timestamp where the signal violated the threshold and the time the signal returned to the nominal voltage level. With the welding speed v_s the length of the detected contaminated segment is calculated. A safety margin s_{SF} is added to ensure a coverage of the entire contaminated segment by the jump distance.

For the demonstrated proof of concept, an IPG YLS AMB 6000/9000 laser with the overall laser power set to 6200 W was used. While the welding speed was 12 m/min, the correction speed to catch up to the nominal spot position was set to 2 m/min, resulting in an overall welding speed of 14 m/min during the repair welding phase. The contamination used for

this demonstration was a small wood splinter within the joint gap. Both sheets consisted of 2.4068 nickel while the face sheet had a thickness of 0.8 mm and the web sheet a thickness of 1.5 mm.

3. Results & Discussion

Using the previously produced specimens containing provoked imperfections of Krämer et al. (Krämer et al. 2024), the influence of rewelding defected seam segments was investigated. As Fig. 2 displays, the previously existing large pores are completely eliminated for defect 1. In the case of the second defect zone, a single small pore remains within the repaired seam, however the overall seam quality was improved significantly, showing good agreement with the observations made by Zhao et al (Zhao and Debroy 2001). Due to the keyhole of the rewelding process interacting with the already existing pores, these likely got incorporated into the vapor flow similar to oscillating welding strategies as described by Fetzer et al. (Fetzer et al. 2018). Furthermore, the CT-scans indicate that the seam underfill got reduced. Judging from the gathered OCT data, the desired keyhole depth could be achieved.

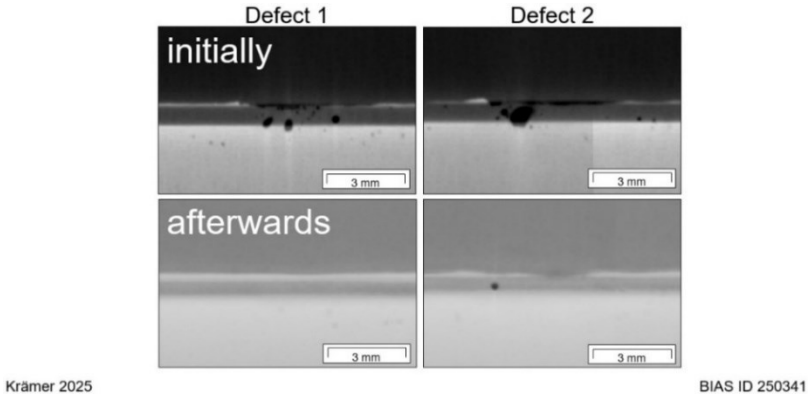

Fig. 2: CT-scans of the same imperfected seam segments before and after rewelding

Based on the findings of the significant improvements on the seam quality by rewelding, the previously described controller system was realized in order to react to detected seam imperfections and demonstrate an in-situ closed loop rewelding approach. In Fig. 3 the corresponding signals of the proof of concept demonstration are displayed.

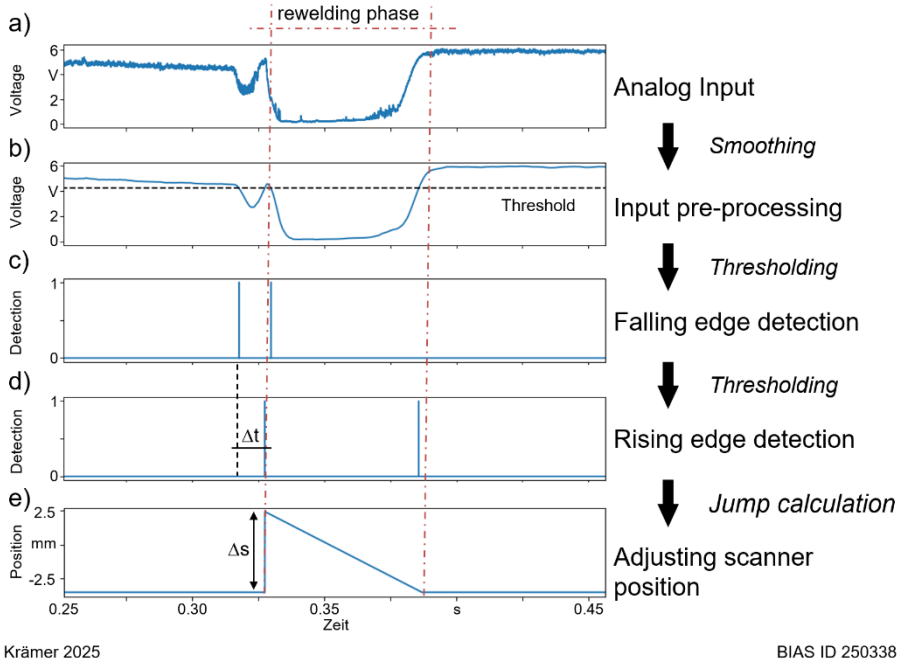

Fig. 3: Data processing and controller intervention with a) analogue pyrometric voltage signal, b) smoothed pyrometric signal, c) negative threshold violation, d) positive threshold violation e) scanner deflection

Fig. 3 a) shows the raw pyrometric analog voltage signal, while Fig. 3 b) shows the smoothed pyrometric signal. A steady decrease in voltage can be observed until the process zone reaches the entrapped wood splinter. Then the signal drops on a short timescale. The violation of the threshold during this drop gets detected by the falling edge detection in Fig. 3 c), while the rising threshold violation detection is displayed in Fig. 3 d). As soon as the signal again rises above the threshold, Δt and subsequently Δs are calculated. The scanner deflects the spot accordingly. The spot deflection in relation to the center point is plotted in Fig. 3 e). The position shifts linearly towards the nominal position due to the constant correction speed. During this rewelding phase, the controller neglects further threshold violations until the nominal position is reached once again. This is necessary as it becomes obvious during the rewelding phase. As the laser spot jumps behind the nominal position, a sudden drop in the pyrometric signal is observed since the process zone is now well behind the measurement spot of the pyrometer, as can be seen in Fig. 4. This results in another falling edge detection as well as a rising edge detection when the process zone again reaches the pyrometric measurement spot. Without this logic of intervention, the controller would deflect the laser spot once more, resulting in a loop of undesired interventions.

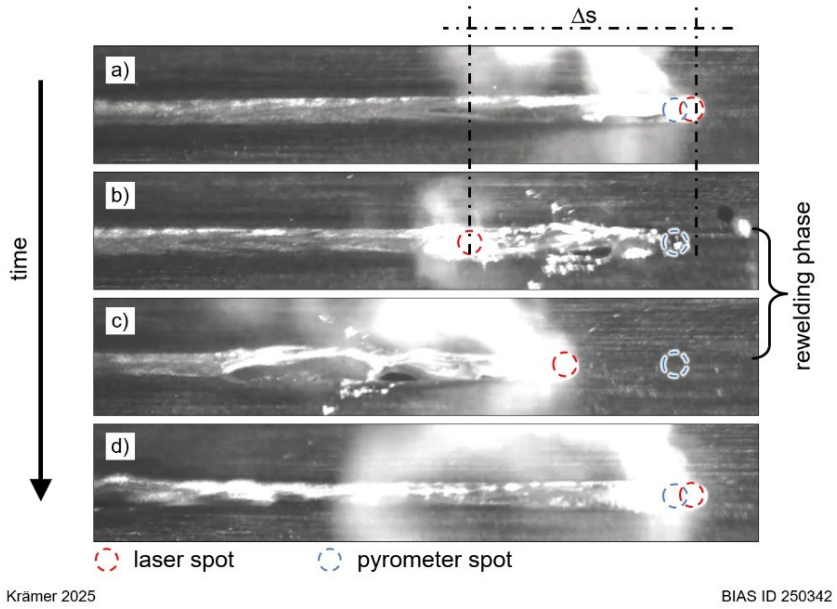

Fig. 4: Single frames of the highspeed imaging during the in-situ rewelding with the laser spot being a) in initial position, b) deflected by the jump distance, c) in the catch-up phase and d) back at the initial position

In Fig. 4 a) a tear in the melt pool is visible. As the controller intervenes and deflects the laser spot, spatters get ejected. This is because the laser power was not shut off during this proof of concept. As Fig. 4 c) shows, the previously existing gap in the seam got reduced during the rewelding phase. There clearly are still some seam defects visible. To prevent those, the repair strategy needs to be improved and adapted, depending on the detected imperfection, which however was not within the scope of this demonstration but will be part of further investigations. Finally, in Fig. 4 d) the nominal laser spot position was reached once again, and the conventional, stable process can be observed. The corresponding highspeed imaging itself was also published as research data (Krämer et al. 2025).

4. Summary

In this work, the possibility of improving the seam quality by rewelding seam areas exhibiting imperfections was demonstrated. Furthermore, due to the sensor based automatic detection of process anomalies based on contaminations within the joint gap of hidden T-joints, a controller was set up for a closed loop automatic in-situ rewelding approach. The functionality of this system and the intervention possibility of this approach were successfully proven.

Acknowledgements

The project on which this publication is based was funded by the German Federal Ministry of Research, Technology and Space under the grant number 03HY119F. The responsibility for the content of the publication lies with the authors.

Federal Ministry of Research, Technology and Space

References

Fetzer, F., Sommer, M., Weber, R., Weberpals, J.-P., Graf, T., 2018. Reduction of pores by means of laser beam oscillation during remote welding of AlMgSi. Optics and Lasers in Engineering 108, pp. 68–77.

Geiger, M., Kägeler, C., Schmidt, M., 2008. High-power laser welding of contaminated steel sheets. Prod. Eng. Res. Devel. 2 (3), pp. 235–240.

Hagenlocher, C., Lind, J., Weber, R., Graf, T., 2020. High-Speed X-Ray Investigation of Pore Formation during Full Penetration Laser Beam Welding of AA6016 Aluminum Sheets Contaminated with Lubricants. Applied Sciences 10 (6), p. 2077.

Krämer, Andreas; Ahlers, Timon; Pordzik, Ronald; Radel, Tim (2025), “Highspeed footage of an automated inline rewelding process based on detection of process anomalies during laser deep penetration welding”, Mendeley Data, V1, doi: 10.17632/tfj4sdmh6y.1

Krämer, A., Henze, I., Pordzik, R., Radel, T., 2024. Inline detection of process anomalies during laser deep penetration welding of hidden T-joints. Procedia CIRP 124, pp. 526–529.

Möbus, M., Pordzik, R., Seefeld, T., 2024. Influence of intensity distributions on the process dynamics during laser deep penetration welding of pure nickel with a flexible ring mode laser source. Journal of Laser Applications 36 (4), Article 042073.

Rathmann, L., Beste, L. H., Faue, P. J., Richter, B., Klingbeil, K., Radel, T., Pfefferkorn, F. E., 2022. Macro-pore free sub-surface PBF-LB/M components through laser polishing. Proceedings of the 12th Laser Applications Forum, Strahltechnik 76.

Yasa, E., Kruth, J.-P., 2011. Microstructural investigation of Selective Laser Melting 316L stainless steel parts exposed to laser re-melting. Procedia Engineering 19, pp. 389–395.

Zhao, H., Debroy, T., 2001. Pore formation during laser beam welding of die-cast magnesium alloy AM60B - Mechanism and remedy. Welding Journal (Miami, Fla) 80, pp. 204–210.